Japanese Journal of Applied Physics **55**, 04EB02 (2016)
http://doi.org/10.7567/JJAP.55.04EB02

REGULAR PAPER

C-atom-induced bandgap modulation in two-dimensional (100) silicon carbon alloys

Tomohisa Mizuno[1]*, Yoshiki Nagamine[1], Yuhsuke Omata[1], Yuhya Suzuki[1], Wako Urayama[1], Takashi Aoki[1], and Toshiyuki Sameshima[2]

[1]*Department of Science, Kanagawa University, Hiratsuka, Kanagawa 259-1293, Japan*
[2]*Department of Engineering, Tokyo University of Agriculture and Technology, Koganei, Tokyo 184-8588, Japan*

*E-mail: mizuno@info.kanagawa-u.ac.jp

Received September 21, 2015; revised November 30, 2015; accepted December 8, 2015; published online March 3, 2016

We experimentally studied the effects of the C atom on bandgap E_G modulation in two-dimensional (2D) silicon carbon alloys, $Si_{1-Y}C_Y$, fabricated by hot C^+ ion implantation into the (100) SOI substrate in a wide range of Y ($4 \times 10^{-5} \leq Y \leq 0.13$), in comparison with the characteristics of 3D silicon carbide (SiC). X-ray photoelectron spectroscopy (XPS) and UV-Raman analysis confirm the Si–C, C–C, and Si–Si bonds in the 2D-$Si_{1-Y}C_Y$ layer. The photoluminescence (PL) method shows that the E_G and PL intensity I_{PL} of 2D-$Si_{1-Y}C_Y$ drastically increase with increasing Y for high Y ($\geq$0.005), and thus we demonstrated a high E_G of 2.5 eV and a visible wavelength λ_{PL} less than 500 nm. Even for low Y ($<10^{-3}$), I_{PL} of 2D-$Si_{1-Y}C_Y$ also increases with increasing Y, owing to the compressive strain of the 2D-$Si_{1-Y}C_Y$ layer caused by the C atoms, but the Y dependence of E_G is very small. E_G of 2D-$Si_{1-Y}C_Y$ can be controlled by changing Y. Thus, the 2D-$Si_{1-Y}C_Y$ technique is very promising for new E_G engineering of future high-performance CMOS and Si photonics. © 2016 The Japan Society of Applied Physics

1. Introduction

Two-dimensional (2D) Si layers are key structures for realizing future CMOS devices, such as extremely thin silicon-on-insulator (ETSOI) and FinFET CMOS,[1,2] as well as Si photonic devices.[3–5] We experimentally demonstrated strong quantum confinement effects (QCEs) in the 2D-Si.[6–11] Namely, Raman spectroscopy showed asymmetrical broadening of Raman spectra even in (100)- and (110)-surface 2D-Si owing to phonon confinement effects (PCEs) caused by Heisenberg's uncertainty principle of the phonon wave vector in a finite Si thickness d_S.[12–15] In addition, the number of Si atom layers of 2D-Si N_L, defined by $N_L \equiv d_S/d + 1$ [d is the distance between two Si atom layers and is 0.136 nm ($\equiv a_S/4$; a_S is the lattice constant of Si) in the case of (100) Si], is a better indicator for evaluating the QCEs of 2D-Si.[7] Both the QCEs of 2D electrons[16–18] and PCEs[19] of 2D-Si cause a reduction in the electron mobility, which is a demerit of the 2D-Si. In addition, the QCEs modulate the energy-band structures of 2D-Si[20–22] and modulate the Si crystals into a direct-bandgap material from indirect-bandgap 3D-Si.[4,19,20,23] Thus, it is possible to evaluate the bandgap (E_G) expansion due to 2D electron confinement effects by the photoluminescence (PL) method. However, in a Si quantum well structure (SQW) of surface-SiO_2/2D-Si/BOX (buried oxide layer in SOI), the 2D-Si layer with thick surface oxide is stressed by a thermal expansion/contraction mismatch between 2D-Si and surface oxide layers during an oxide layer formation process,[11,24,25] because the linear coefficient of thermal expansion of Si, α_S, is about 5 times as large as that of oxide, α_{OX}.[26] We experimentally confirmed the tensile strain dependence of the PL peak photon energy E_{PH} of the (100)2D-Si layer by UV-Raman spectroscopy[11] and that E_{PH} under the fully relaxed condition agrees well with the theoretical E_G by the first-principles calculation of 2D-Si with a surface terminated by the H atoms.[20] Thus, we assume that E_G of (100)2D-Si can be precisely evaluated by the E_{PH} value.[11] However, a wide FWHM (~0.3 eV) of the PL spectrum in the 2D-Si cannot at present be simply explained only by the direct transmission of electrons from the conduction to valence bands and the 2D-Si thickness variations,[11] and thus the detailed analysis of PL spectra is still required.

E_G of (100)2D-Si can be controlled by d_S,[9,20] but is still lower than 1.9 eV. As a result, the peak PL photon wavelength λ_{PL} is longer than 650 nm.[11] Therefore, to realize a high-speed source heterojunction transistor (SHOT), which can inject high-velocity carriers into a channel with low E_G from high-E_G source regions, using the band offset energy at the source heterojunction,[27–29] it is necessary to develop a new technology for realizing higher E_G without controlling d_S. It is possible that the higher E_G engineering is also suitable for visible Si photonics. Actually, in 3D-$Si_{1-Y}C_Y$, E_G can increase with increasing Y,[30–32] and the PL intensity I_{PL} also increases with increasing Y.[30] Therefore, 2D-$Si_{1-Y}C_Y$ is a candidate for new E_G and λ_{PL} engineering for future CMOS and Si-photonics.

In this work, we experimentally studied the impact of Y on E_G modulation of 2D-$Si_{1-Y}C_Y$[33] with a wide range of Y, fabricated by the $^{12}C^+$ hot ion-implantation technique into (100)SOIs at 900 °C,[34] where Y was evaluated by secondary ion mass spectrometry (SIMS) analysis and X-ray photoelectron spectroscopy (XPS), resulting in $10^{-5} < Y \leq 0.13$ in this study. The minimum N_L of 2D-$Si_{1-Y}C_Y$ is 4 in this study, which is smaller than that of the Si unit cell, 5. We confirmed the bonds of Si and Si (Si–Si), of Si and C (Si–C), and of C and C (C–C) in 2D-$Si_{1-Y}C_Y$ by XPS and UV-Raman spectroscopy, and thus 2D-$Si_{1-Y}C_Y$ was successfully formed. By the PL method with an excitation laser energy E_{EX} from 2.3 to 3.8 eV, we experimentally verified that E_{PH} of 2D-$Si_{1-Y}C_Y$ rapidly increases with increasing Y, and demonstrated E_{PH} higher than 2.5 eV and visible λ_{PL} around 500 nm.

2. Experiment procedure for 2D-$Si_{1-Y}C_Y$ by hot C^+ ion implantation technique

Figure 1 shows the fabrication steps for 2D-$Si_{1-Y}C_Y$ layers using 55-nm thick (100) bonded SOI substrates with the BOX thickness of 145 nm.[35] High-quality 2D-$Si_{1-Y}C_Y$ layers with a wide range of Y were fabricated by the combination of 1) $^{12}C^+$ hot ion implantation[34] and 2) two-step dry thermal oxidation.[33] $^{12}C^+$ hot ion implantation into the 8.5-nm-thick (100) bonded SOI substrate[35] was carried out at the SOI substrate temperature of 900 °C, as shown in Fig. 1(b), after thinning the Si layer by high-T (1000 °C) oxidation of initial SOI substrate shown in Fig. 1(a). Figure 1(c) shows that the

 © 2016 The Japan Society of Applied Physics

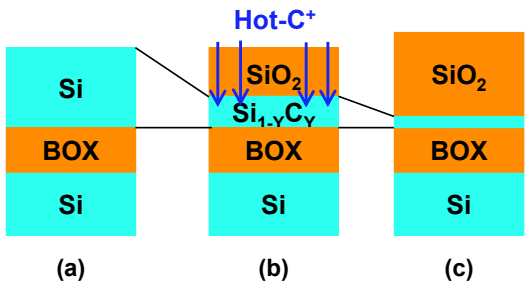

Fig. 1. (Color online) Schematic fabrication steps for 2D-$Si_{1-Y}C_Y$ layers. (b) Hot $^{12}C^+$ ion implantation into 8.5-nm-thick (100)SOI substrate at 900 °C was carried out after (a) 1000 °C dry oxidation of initial 55-nm-thick SOI. D_C was varied from 5×10^{12} to $2 \times 10^{16}\,cm^{-2}$ at $E_A = 32$ keV. (c) Additional 900 °C dry oxidation was carried out for thinning $Si_{1-Y}C_Y$ layers. In this study, $10^{-5} < Y \leq 0.13$, and the minimum N_L was 4.

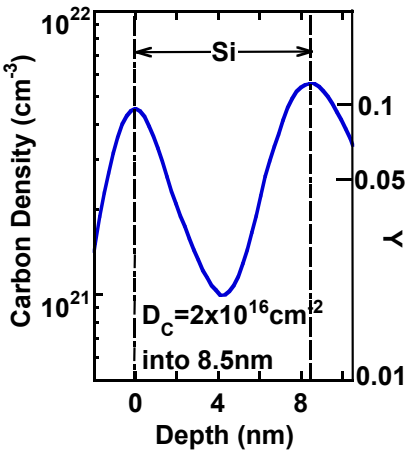

Fig. 2. (Color online) SIMS results of N_C (solid line) just after hot C^+ ion implantation into 8.5-nm-thick SOI, which has the minimum thickness for SIMS measurement, where D_C is $2 \times 10^{16}\,cm^{-2}$. C atoms are localized at both the surface-SiO_2 and BOX interfaces; the peak concentration is about $5.6 \times 10^{21}\,cm^{-3}$ at the BOX interface. This N_C results in $Y = 0.13$ (right axis). SIMS accuracy at the Si/BOX interface is about 60%.

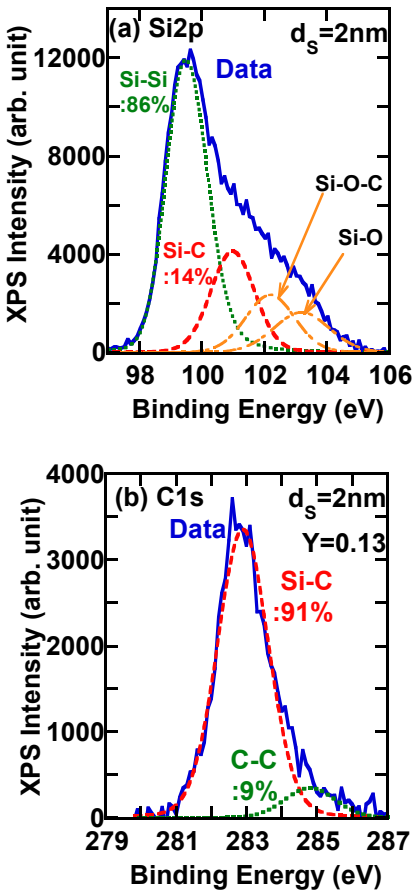

Fig. 3. (Color online) XPS data of (a) Si-2p and (b) C-1s spectra in $Si_{1-Y}C_Y$ layers, where $D_C = 2 \times 10^{16}\,cm^{-2}$ and $d_S = 2$ nm. The solid, dotted, dashed, and dot-dash lines in (a) show the experimental data, and the fitted curves for Si–Si, Si–C, and SiO_X bonds, respectively. The solid, dashed, and dotted lines in (b) show the experimental data, and the fitted curves for Si–C and C–C bonds, respectively. (a) shows that about 14% of Si atoms bind to C atoms. (b) shows that about 91% of C atoms bind to Si atoms.

2D-$Si_{1-Y}C_Y$ layers were subsequently formed by the low-T (900 °C) oxidation process. Y was controlled by the $^{12}C^+$ ion dose D_C, where D_C was varied from 5×10^{12} to $2 \times 10^{16}\,cm^{-2}$ at the $^{12}C^+$ ion energy of 32 keV whose projection range is the middle of the Si layer. The minimum N_L (d_S) of 2D-$Si_{1-Y}C_Y$, evaluated by the UV–visual reflection method,[6] was 4 (0.4 nm) in this work, which is smaller than that of Si unit cell, 5. The surface oxide thickness T_{OX} after the process in Fig. 1(c) was about 120 nm. In this study, we analyzed the physical properties of the $Si_{1-Y}C_Y$ layer with the surface oxide, whose structure is the surface-oxide/Si/BOX SQW.

In the case of relatively thick $Si_{1-Y}C_Y$, the C concentration N_C of the $Si_{1-Y}C_Y$ layer can be analyzed by SIMS, where the incident ion is Cs^+ with an acceleration voltage of 1 kV and the measurement area is 7100 μm^2. Figure 2 shows the SIMS result for the N_C depth profile in 8.5 nm $Si_{1-Y}C_Y$ just after the $^{12}C^+$ hot ion implantation shown in Fig. 1(b), where D_C is the maximum value of $2 \times 10^{16}\,cm^{-2}$ in this study. The depth accuracy for SIMS is about 2 nm. The error of the C concentration is about 40%, but increases to about 60% at the Si interface. C atoms are not uniformly distributed in the $Si_{1-Y}C_Y$ layer, and condenses locally at the two interfaces of the BOX and surface SiO_2 with the FWHM of about 3 nm, because of redistribution effects of C atoms during hot ion implantation. The maximum N_C is about $5.6 \times 10^{21}\,cm^{-3}$ at the BOX interface, resulting in $Y \approx 0.13$.

On the other hand, in the case of very thin $Si_{1-Y}C_Y$, the C depth profile and the composition of the bonds of Si and Si atoms (Si–Si), Si and C atoms (Si–C), and C and C atoms (C–C) can also be analyzed by XPS with a thickness detection limit of about 2 nm. Figures 3(a) and 3(b) show the experimental data (solid lines) of Si-2p and C-1s spectra in the thinned $Si_{1-Y}C_Y$ layer with $d_S = 2$ nm, respectively, where D_C is $2 \times 10^{16}\,cm^{-2}$. The experimental data of the Si-2p spectrum can be fitted by the Si–Si (dotted line), Si–C (dashed line), and Si–O_x bonds (dotted and dashed lines). The C-1s spectrum can also be fitted by the Si–C (dashed line) and C–C bonds (dotted line), but there are no C–O_x bonds. Since XPS can detect the atomic spectrum within a depth of about 4 nm, Si–O_x and Si–C–O bond intensities in Fig. 3(a) are attributable to the XPS spectra of SiO_2 layers at the surface and BOX sides. Using the fitting curve areas of the Si–Si and Si–C bond peaks in Fig. 3(a), about 86 and 14% of Si atoms bind to Si and C atoms, respectively. In addition, the C-1s spectrum in Fig. 3(b) shows that about 91 and 9% of C atoms bind to the Si and C atoms, respectively. Thus, the C–C bond suggests that 9% of all C atoms separates out in the Si layer at $Y = 0.13$. Consequently, we experimentally

© 2016 The Japan Society of Applied Physics

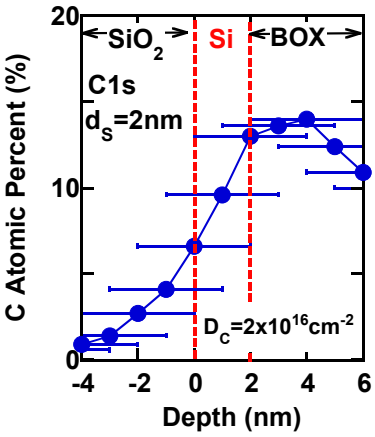

Fig. 4. (Color online) Depth profile of C atomic percent obtained using depth dependence of XPS C-1s spectrum of 2D-$Si_{1-Y}C_Y$ layers, where $D_C = 2 \times 10^{16}\,cm^{-2}$ and $d_S = 2\,nm$. Lateral error bars are about 4 nm, because of the penetration depth of X-ray in $Si_{1-Y}C_Y$ layers. The maximum C atomic percent at the BOX interface is about 13%, which agrees with SIMS data of C concentration (0.13) at the BOX interface in 8.5-nm-thick $Si_{1-Y}C_Y$ shown in Fig. 2(a). Thus, the C atomic percent at the BOX interface is almost independent of d_S.

confirmed three regions of Si, Si–C, and C in the $Si_{1-Y}C_Y$ alloy layer in this study. From the C 13 at. % in the $Si_{1-Y}C_Y$ layer determined from the C-1s spectrum at $D_C = 2 \times 10^{16}\,cm^{-2}$ shown in Fig. 3(b), it can be estimated that 12 at. % of C atoms binds to Si atoms (Si–C), whereas only 1 at. % of C atoms separates out in the Si layer. In addition, it is also possible that some part of the separated C atoms exists in the Si interstitial.

Using the depth dependence of the C-1s spectrum of XPS, the C atomic percent profile of $Si_{1-Y}C_Y$ can be obtained even at $d_S = 2\,nm$. Figure 4 shows the C atomic percent profile of $Si_{1-Y}C_Y$ with the XPS lateral error bar of 4 nm, where $D_C = 2 \times 10^{16}\,cm^{-2}$. It is also confirmed by XPS that C atoms are localized at the BOX interface, but we observed no C atom peak at the surface oxide interface as shown in the SIMS data $d_S = 8.5\,nm$ (Fig. 2). The C atom profile change from 8.5 to 2 nm of d_S is possibly attributable to the following mechanism. During the oxidation process [Fig. 1(c)] after C^+ implantation, the surface-oxide/Si interface edge shifts to the inner part of the Si layer, and then the localized C atoms at the Si surface diffuse to the surface oxide. On the other hand, the maximum C atomic percent at the BOX interface at $d_S = 2\,nm$ is about 13%, which agrees with the maximum C concentration at the BOX interface (0.13) in the case of $d_S = 8.5\,nm$ shown in Fig. 2. Thus, Figs. 2 and 4 indicate that the maximum Y at the BOX interface in $Si_{1-Y}C_Y$ is independent of N_L (d_S), since the BOX interface edge does not shift even during the 900 °C oxidation process, and thus the C atom peak at the BOX interface still remains. Therefore, we can assume $Y \approx 0.13$ even at $N_L = 4$ in the case of $D_C = 2 \times 10^{16}\,cm^{-2}$. Generally, the implanted impurity concentration is proportional to the ion dose. Thus, using $Y \approx 0.13$ at $D_C = 2 \times 10^{16}\,cm^{-2}$, we can determine Y in 0.4 nm $Si_{1-Y}C_Y$ as a function of D_C in this study as

$$Y = 6.5 \times 10^{-18} D_C. \quad (1)$$

Therefore, 2D-$Si_{1-Y}C_Y$ layers with a wide range of $4 \times 10^{-5} \leq Y \leq 0.13$ were successfully formed by changing D_C

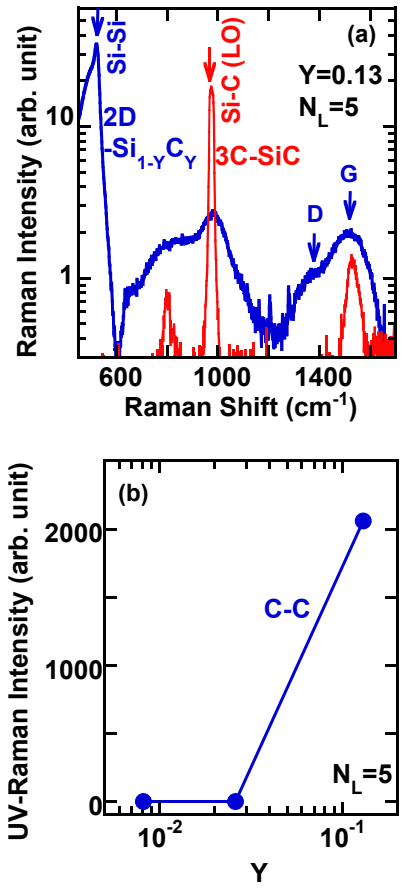

Fig. 5. (Color online) (a) UV-Raman spectra of 2D-$Si_{0.87}C_{0.13}$ (blue line) and bulk 3C-SiC (red line), where $N_L = 5$. Raman peak at 970 cm^{-1} is the LO mode of Si–C vibration,[35] which agrees with that of 3C-SiC. Double Raman peaks of 2D-$Si_{0.87}C_{0.13}$ at around 1500 cm^{-1} are attributable to D (1340 cm^{-1}) and G (1500 cm^{-1}) vibrational modes of graphitic C.[36] (b) Raman intensity at G vibrational mode of 1500 cm^{-1} peak as a function of Y. We can detect the G mode peak only for $Y = 0.13$ and there is no G mode peak for $Y \leq 0.016$.

in this work. Consequently, the physical properties of 2D silicon carbon alloy comprise the physical properties of the three regions of 2D-Si, Si–C, and separated C layers.

Moreover, Fig. 5(a) shows UV-Raman spectra of 2D-$Si_{0.87}C_{0.13}$ (blue line) and bulk 3C-SiC (red line), where the Raman excitation laser wavelength was 325 nm and $N_L = 5$. The maximum Raman intensity of 2D-$Si_{0.87}C_{0.13}$ is the Si–Si vibration mode at 520 cm^{-1}. The Raman peak at 970 cm^{-1} of 2D-$Si_{0.87}C_{0.13}$ is the LO mode of Si–C vibration,[36] which agrees with that of 3C-SiC. Moreover, the Raman peak at 970 cm^{-1} of the Si–C vibration mode can also be observed when $Y \geq 0.5\%$. Thus, we also confirmed the Si–C bond by Raman spectroscopy for $Y \geq 0.5\%$. In addition, double Raman peaks of 2D-$Si_{0.87}C_{0.13}$ at around 1500 cm^{-1} are attributable to D (1340 cm^{-1}) and G (1500 cm^{-1}) bands of graphitic C,[36] which is due to the C atoms originating from the separation of C–C bonds, as evaluated by the C-1s spectrum shown in Fig. 3(b). The G band is also observed in 3C-SiC. The Y dependence of the C atom separated in 2D-$Si_{1-Y}C_Y$ can be estimated from the graphitic C vibration peak in Fig. 5(a) and is shown in Fig. 5(b). The graphitic C peak is observed only at $Y = 0.13$, and we cannot observe the C–C peak when $Y \leq 0.016$. Thus, the C atoms do not separate out

© 2016 The Japan Society of Applied Physics

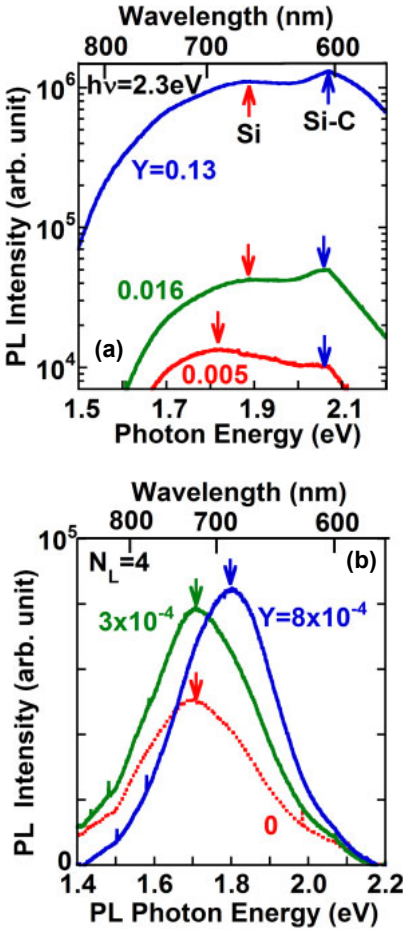

Fig. 6. (Color online) PL spectra excited by 2.3 eV laser as a function of Y for (a) high Y (≥ 0.005) and (b) low Y ($< 10^{-3}$), where $N_L = 4$. Lower and upper axes show PL photon energy and wavelength, respectively. The dotted line in (b) shows the PL spectrum of intrinsic 2D-Si. (a) shows that double PL peaks are newly observed. Arrows in (a) show peak I_{PL} attributable to Si and Si–C regions. Under both Y conditions, I_{PL} rapidly increases with increasing Y.

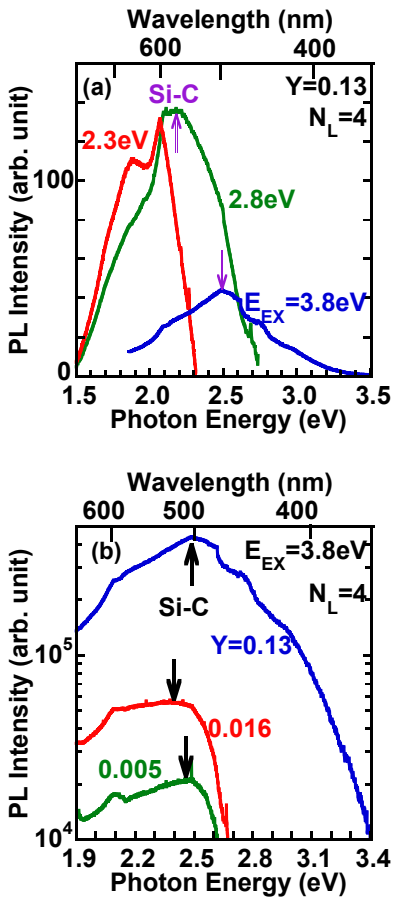

Fig. 7. (Color online) 2D-$Si_{1-Y}C_Y$ PL results of (a) excitation laser energy dependence of PL spectra at $Y = 0.13$, and (b) Y dependence of PL spectra excited by 3.8 eV laser, where $N_L = 4$. Blue, green, and red lines in (a) show the data excited by E_{EX} of 3.8, 2.8, and 2.3 eV, respectively. When $E_{EX} = 3.8$ eV, PL spectrum of 2D-$Si_{0.87}C_{0.13}$ with $E_{PH} > 3$ eV can be accurately observed because $E_G < E_{EX}$. (b) shows that all spectra show non-Gaussian curves and I_{PL} even in the visible region rapidly increases with increasing Y.

in 2D-$Si_{1-Y}C_Y$ when $Y \leq 0.016$, and the C phase separation in 2D-$Si_{1-Y}C_Y$ occurs only at a high Y of 0.13.

Furthermore, we observed no degradation of the FWHM of the Si Raman peak of 8.5-nm-thick $Si_{1-Y}C_Y$ layers just after hot C^+ ion implantation in the range of $5 \times 10^{12} \leq D_C \leq 2 \times 10^{16}\,cm^{-2}$, compared with the FWHM of Si bulk, which is the benefit of the hot C^+ ion-implantation technique. Thus, since the FWHM is an indicator of the crystal quality, the hot C^+ ion-implantation-induced damage of the Si layer is considered to be very small in this study. As a result, PL properties are not degraded by the electron lifetime reduction due to Si crystal damage. Moreover, in the case of SHOT, the crystal quality of the source region composed of $Si_{1-Y}C_Y$ is not also degraded by the hot C^+ ion implantation.

In this study, we mainly analyzed the E_G properties of 2D-$Si_{1-Y}C_Y$ layers at N_L of about 4, by the PL method at room temperature, where the excitation laser energy E_{EX} varied from 2.3 to 3.8 eV. As references, three types of 3D silicon carbide (SiC) (3C-, 4H-, and 6H-SiC) were also measured. The excitation laser power P_L was set to be 1 mW to suppress the P_L heating effects on Si,[7] and the laser diameter was 1 μm.

3. Experimental results and discussion

3.1 C-atom-induced bandgap modulation

Since there are three regions composed of Si, Si–C, and C in 2D-$Si_{1-Y}C_Y$ layers, as revealed by XPS and Raman analyses, both PL and Raman intensities of 2D-$Si_{1-Y}C_Y$ are considered to be the sum of the intensities of the three regions of Si, Si–C, and separated C regions.

Figures 6(a) and 6(b) show the PL spectra of 2D-$Si_{1-Y}C_Y$ layers excited by E_{EX} of 2.3 eV under high-Y ($\geq$0.005) and low-Y ($<10^{-3}$) conditions, respectively, where $N_L = 4$. Under high-Y conditions ($\geq$0.005) where Si–C and C–C bonds are confirmed by XPS and UV-Raman spectroscopy, Fig. 6(a) shows that very strong and double-peak PL spectra can be newly observed even when $0.005 \leq Y \leq 0.016$ where there is no C–C Raman peak in Fig. 5(b). Therefore, it is considered that the influence of the separated C atoms at $Y = 0.13$ on the double PL peaks is not so large in this study. As a result, the first lower and second higher E_{PH} are considered to be attributable to 2D-Si and Si–C regions, respectively, and the 1st E_{PH} increases with increasing Y when $Y \geq 0.016$. The new 2nd higher E_{PH} is considered to be PL from the 2D Si–C region, which will be discussed in detail, as shown in Fig. 7. I_{PL} of the Si peak of the Si region drastically increases with

© 2016 The Japan Society of Applied Physics

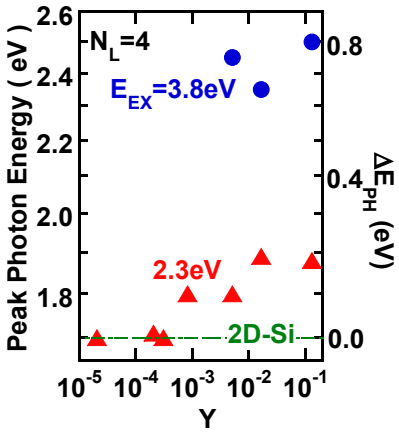

Fig. 8. (Color online) Y dependence of E_{PH} excited by E_{EX} of 3.8 (circles) and 2.3 eV (triangles), where $N_L = 4$. The right vertical axis shows the E_G shift of 2D $Si_{1-Y}C_Y$ compared with the E_G of 2D-Si (dot-dash line), ΔE_G. ΔE_G at E_{EX} of 3.8 eV is much larger than that at E_{EX} of 2.3 eV, and the former is independent of Y, whereas the latter depends on Y.

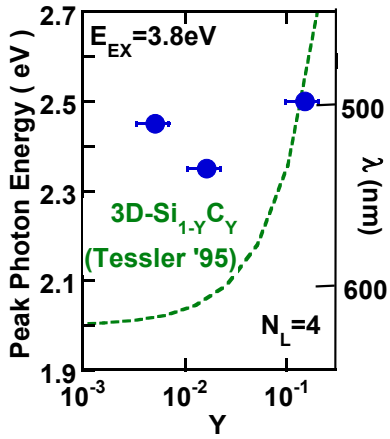

Fig. 9. (Color online) Y dependence of E_{PH} (left axis) and peak λ_{PL} (right axis) of Si–C region (circles), where $E_{EX} = 3.8$ eV and $N_L = 4$. E_{PH} is nearly independent of Y. Dashed line shows the data of 3D-$Si_{1-Y}C_Y$ by Tessler et al.,[30] and E_{PH} only at $Y = 0.13$ is almost the same as that in the 3D-$Si_{1-Y}C_Y$.

increasing Y when $Y \geq 0.005$. On the other hand, under low-Y conditions ($\leq 8 \times 10^{-4}$) shown in Fig. 6(b), the PL spectrum has the usual single-peak shape attributable to the 2D-Si region,[7] and I_{PL} also increases with increasing Y, compared with that of intrinsic 2D-Si (dotted line). Moreover, E_{PH} also increases only at $Y = 8 \times 10^{-4}$.

Here, we discuss the E_{EX} dependence of the PL spectrum of 2D-$Si_{0.87}C_{0.13}$, because PL photons higher than about 2 eV cannot be detected at E_{EX} of 2.3 eV. Figures 7(a) and 7(b) show the E_{EX} dependence of the PL spectra of 2D-$Si_{0.87}C_{0.13}$ at photon energies higher than 2 eV and the Y dependence of the PL spectrum excited by 3.8 eV laser, respectively, where $N_L = 4$. As shown in Fig. 7(a), the PL spectrum of 2D-$Si_{0.87}C_{0.13}$ in the visible region strongly depends on E_{EX}, and I_{PL} for in energy higher than 2.4 eV drastically increases at the 3.8 eV laser, because electrons can be generated under the condition of $E_G \leq E_{EX}$. When $E_{EX} = 3.8$ eV, we can newly observe a PL spectrum at $Y = 0.13$ with photon energy higher than 2 eV; it has a complicated shape with many peaks, compared with the usual Gaussian shape of PL spectrum shown in Fig. 6(b) for low Y. This complicated PL shape cannot be explained at present. The peak E_{PH} reaches 2.5 eV at $E_{EX} = 3.8$ eV, resulting in $\lambda_{PL} \approx 500$ nm. The PL spectrum tail with higher than 3 eV can also be detected. However, the clear PL peak at 1.9 eV excited by the 2.3 eV laser (red line) cannot be observed when using the 3.8 eV laser, which suggests that the PL peak cannot be detected under the condition of $E_G \ll E_{EX}$. Thus, E_{EX} should be optimized for PL measurement. On the other hand, Fig. 7(b) shows that the peak E_{PH} is almost independent of Y, but the PL spectrum tail at higher photon energy drastically increases with increasing Y. Thus, the higher photon energy component of the PL spectrum (>2.5 eV) strongly depends on Y.

Here, Fig. 8 shows the Y dependence of the 1st E_{PH} at $E_{EX} = 2.3$ eV (triangles) shown in Fig. 6 and E_{PH} at $E_{EX} = 3.8$ eV (circles) shown in Fig. 7(b), where $N_L = 4$. The right vertical axis shows the E_{PH} enhancement of 2D-$Si_{1-Y}C_Y$, ΔE_{PH}, compared with E_{PH} of intrinsic 2D-Si (dotted and dashed line). For $Y \geq 0.005$, a large ΔE_{PH} of about 0.8 eV (E_{PH} of about 2.5 eV) can be achieved at $E_{EX} = 3.8$ eV, but it is nearly independent of Y. On the other hand, in the case of $E_{EX} = 2.3$ eV, E_{PH} gradually increases with increasing Y, but is saturated at about 1.9 eV for $Y \geq 0.016$. Thus, ΔE_{PH} at $E_{EX} = 3.8$ eV is much larger than that at $E_{EX} = 2.3$ eV. On the other hand, these E_{PH} saturations at $Y = 0.13$ under both E_{EX} conditions may be due to the C atom separation in Si layer shown in Fig. 5(b).

Consequently, we experimentally verified the bandgap engineering by the 2D-$Si_{1-Y}C_Y$ technique, that is, E_G modulation by C atoms in the 2D-$Si_{1-Y}C_Y$ layer.

3.2 Physical mechanism for bandgap modulation in 2D-$Si_{1-Y}C_Y$

In this subsection, we discuss the physical mechanism behind the Y dependence of E_{PH} in the 2D-$Si_{1-Y}C_Y$ layer shown in Fig. 8.

For the case of high-Y conditions ($0.005 \leq Y \leq 0.13$), Fig. 9 shows E_{PH} of 2D-$Si_{1-Y}C_Y$ (circles) as a function of Y. The dashed line shows E_G of 3D-$Si_{1-Y}C_Y$ reported by Tessler et al.,[30] and E_G of 3D-$Si_{1-Y}C_Y$ rapidly increases with increasing Y when $Y > 0.01$. As a result, E_{PH} of 2D-$Si_{1-Y}C_Y$ only at $Y = 0.13$ is almost the same as E_G of 3D-$Si_{1-Y}C_Y$. Thus, under a higher Y condition of 0.13, the physical mechanism behind the E_{PH} increase of 2D-$Si_{1-Y}C_Y$ is probably similar to that of 3D-$Si_{1-Y}C_Y$ which is attributable to C-atom-induced bandgap modulation (CIBM).[30] The discrepancy between the 2D- and 3D-$Si_{1-Y}C_Y$ with lower Y (< 0.13), which is characteristic of 2D-$Si_{1-Y}C_Y$, is not physically understood at present.

On the other hand, as shown in Fig. 6(b), even with a low Y of 8×10^{-4}, we can observe I_{PL} enhancement ($I_{PL}/I_{PL0} = 1.66$) and E_G expansion ($= 1.8$ eV). However, no 2nd E_{PH} due to the Si–C peak was observed when $Y < 0.001$. Next, we discuss the strain-induced bandgap modulation by C atoms in 2D-$Si_{1-Y}C_Y$ with low Y ($Y < 0.02$).

The lattice constant of 3D-$Si_{1-Y}C_Y$, a_{SC}, is reported to decrease with increasing Y compared with that of 3D-Si, a_S,[32] because of the C atom effects on a_{SC}. Therefore, the compressive strain ε_C even in 2D-$Si_{1-Y}C_Y$ is assumed to obey

© 2016 The Japan Society of Applied Physics

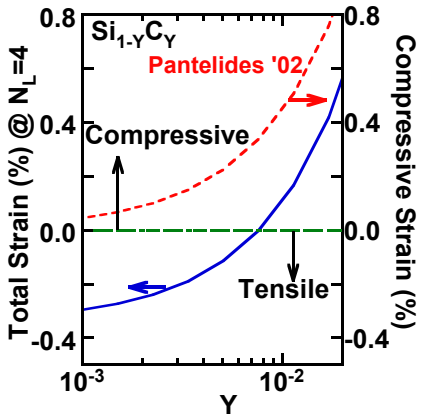

Fig. 10. (Color online) Y dependence of strain (solid line) of $Si_{1-Y}C_Y$ with $N_L = 4$ estimated using Eq. (3) and compressive strain (dashed line) of 3D-$Si_{1-Y}C_Y$ calculated using Eq. (2) by Pantelides et al.[32] The tensile strain can be relaxed by increasing Y.

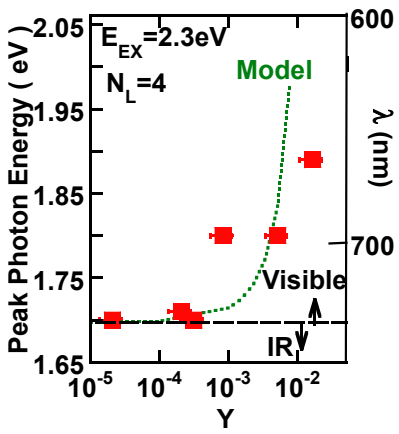

Fig. 11. (Color online) Y dependence of E_{PH} (squares) (left axis) and peak λ_{PL} (right axis), where $E_{EX} = 2.3$ eV and $N_L = 4$. Dotted line shows the tensile strain dependence of E_G model in 2D-$Si_{1-Y}C_Y$ calculated using Eq. (4). Results obtained with Eq. (4) can well explain the experimental data.

Vegard's linear rule, shown as the following equation for 3D-$Si_{1-Y}C_Y$ reported by Pantelides et al.[32]

$$\varepsilon_C(Y) = \frac{a_S - a_{SC}(Y)}{a_S} = \frac{-0.24Y + 0.057Y^2}{a_S} \tag{2}$$

The dashed line in Fig. 10 shows ε_C calculated using Eq. (2); ε_C rapidly increases with increasing Y for $Y > 0.01$.

On the other hand, residual tensile strain ε_T is applied in 2D-Si, because of the large difference in the expansion coefficient between the surface SiO_2 and 2D-Si in the SQW structure.[11] For $N_L = 4$, we already reported that experimental ε_T was about 0.3% in 2D-Si.[11] Thus, total tensile strain $\varepsilon(Y)$ [%] in 2D-$Si_{1-Y}C_Y$ can be expressed as follows, following Eq. (2).

$$\varepsilon(Y) = \varepsilon_T - 100\varepsilon_C(Y) = 0.3 - \frac{-24Y + 5.7Y^2}{a_S} \tag{3}$$

$\varepsilon(Y)$ calculated using Eq. (3) is shown by the solid line in Fig. 10, and the residual tensile strain is relaxed by the compressive strain ε_C expressed by Eq. (2) when $Y < 0.01$.

According to the tensile-strain-induced E_G lowering in 2D-Si evaluated from the surface SiO_2 thickness T_{OX} dependence

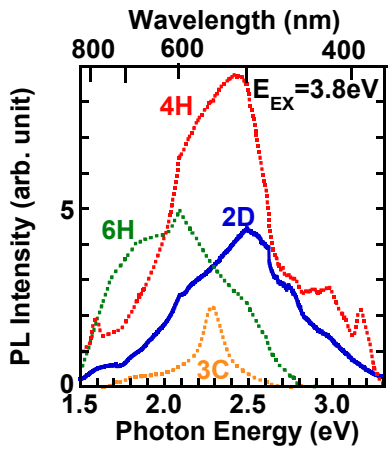

Fig. 12. (Color online) PL spectrum of 2D-$Si_{0.87}C_{0.13}$ (solid line) compared with those of three structure types of bulk silicon carbide, where $N_L = 4$ and E_{EX} is 3.8 eV. Orange, red, and green dotted lines show PL spectra of 3C-, 4H-, and 6H-silicon carbides, respectively. PL spectrum of 2D-$Si_{0.87}C_{0.13}$ is similar to that of 4H-SiC, but is far from that of 3C-SiC with a small FWHM.

of E_{PH} in our previous paper,[11] $E_G(Y)$ of 2D-$Si_{1-Y}C_Y$ depends on $\varepsilon(Y)$ in Eq. (3), and is experimentally fitted by the following equation of $\varepsilon(Y)$.[11]

$$E_G(Y) = E_0 + E_1 \exp\left[-\frac{\varepsilon(Y)}{\varepsilon_0}\right] \tag{4}$$

Here, fitting parameters E_0, E_1, and ε_0 were 1.67 and 0.346 eV, and 0.22% in the case of $N_L = 4$, respectively.[11]

Here, Fig. 11 shows the experimental E_{PH} (λ_{PL}) (squares) shown in Fig. 6 as a function of Y, where $E_{EX} = 2.3$ eV and $N_L = 4$. The dotted line shows the $E_G(Y)$ of 2D-$Si_{1-Y}C_Y$ calculated using Eq. (4), and can well explain the experimental E_{PH} (λ_{PL}) data for $Y < 0.02$. Thus, the E_G increase with increasing Y for $Y < 0.02$ is attributable to the ε_T-relaxation-induced E_G expansion described by Eqs. (3) and (4). Consequently, even small Y (< 0.02) can affect E_G of 2D-$Si_{1-Y}C_Y$.

Consequently, the 2D-$Si_{1-Y}C_Y$ alloy technique is very promising for E_G engineering in SHOT structures and Si photonics.

Finally, we compare the PL spectrum of 2D-$Si_{0.87}C_{0.13}$ with those of three types of 3D silicon carbides (3C-, 4H-, and 6H-SiC), as shown in Fig. 12, where $E_{EX} = 3.8$ eV and N_L of 2D-$Si_{0.87}C_{0.13}$ is 4. Almost all PL intensities, except for that of 3C-SiC are of the same order. The PL spectrum of 2D-$Si_{0.87}C_{0.13}$ is similar to that of 4H-SiC but different from that of 3C-SiC with a small FWHM, but the Si and C atom configuration in 2D-$Si_{0.87}C_{0.13}$ is not yet analyzed in detail.

3.3 PL intensity enhancement in 2D-$Si_{1-Y}C_Y$

Using the results of Figs. 6 and 7(b), Fig. 13(a) shows the Y dependence of the peak I_{PL} of the 1st E_{PH} in 2D-$Si_{1-Y}C_Y$ layers normalized by that of 2D-Si at $Y = 0$, I_{PL0} (dotted line), where $E_{EX} = 2.3$ eV and $N_L = 4$. For $Y < 10^{-3}$, I_{PL}/I_{PL0} slightly increases. However, in the case of double peaks region at $Y = 0.005$ shown in Fig. 6(a), I_{PL}/I_{PL0} suddenly decreases. The physical mechanism is not understood at present. In addition, for $Y \geq 0.005$, I_{PL}/I_{PL0} drastically increases with increasing Y, again. As a result, $I_{PL}/I_{PL0} \propto$

© 2016 The Japan Society of Applied Physics

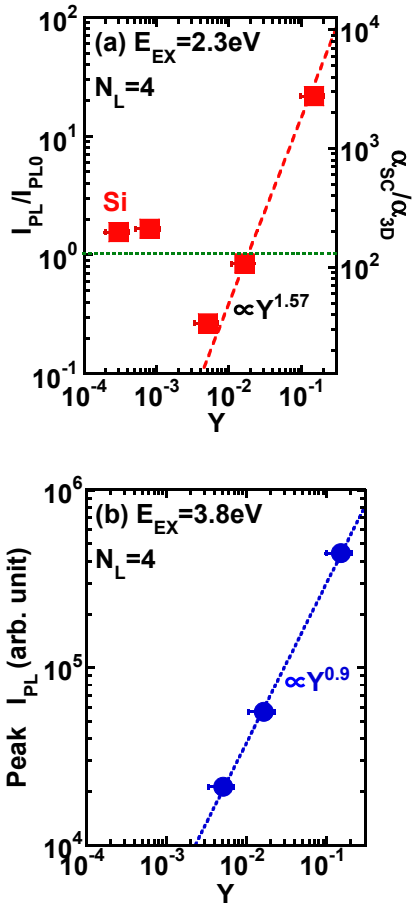

Fig. 13. (Color online) (a) Peak I_{PL} of Si region in 2D-$Si_{1-Y}C_Y$ normalized by that of 2D-Si with $Y = 0$ (dotted line), I_{PL0} vs Y, where E_{EX} is 2.3 eV, and $N_L = 4$. The right axis in (a) shows α_{SC} of 2D-$Si_{1-Y}C_Y$ normalized by α_{3D} of 3D-Si,[37] estimated using Eq. (6). (a) shows that I_{PL}/I_{PL0} drastically increases with increasing Y and can be well fitted by power law of Y, $I_{PL} \propto Y^{1.57}$ (dashed line) when $Y > 10^{-3}$, where the correlation coefficient is about 1. Error bars show the accuracy (35%) of Y obtained by XPS. α_{SC} is about three orders of magnitude higher than α_{3D}. (b) Peak I_{PL} vs Y, where $E_{EX} = 3.8$ eV and $N_L = 4$. (b) also shows $I_{PL} \propto Y^{0.9}$ with the correlation coefficient of about 1.

$Y^{1.57}$ for $Y \geq 0.005$. In particular, I_{PL}/I_{PL0} at $Y = 0.13$ exceeds 20, which is highly suitable for Si photonics. Here, assuming that PL photons are caused by the direct transmission of electrons between the conduction and valence bands, I_{PL} is simply given by[26]

$$I_{PL} \propto \alpha\eta = \alpha\left(1 + \frac{\tau_R}{\tau_{NR}}\right)^{-1}, \tag{5}$$

where α, η, τ_R, and τ_{NR} are the absorption coefficient, luminescence efficiency, and radiative, and nonradiative lifetimes of electrons, respectively. Thus, it is possible that η is modulated in 2D-$Si_{1-Y}C_Y$. However, assuming that η is constant in this study, the I_{PL} increase is probably attributable to the α enhancement. The right axis shows α of 2D-$Si_{1-Y}C_Y$, α_{SC}, compared with that of 3D-Si (α_{3D}) at $E_{EX} = 2.3$ eV.[37] α_{SC} is estimated to be about 26 times as large as that of 2D-Si (α_{2D}), and α_{2D} is two orders of magnitude larger than that of α_{3D}, because the direct bandgap structure of 2D-Si changed from the indirect bandgap of 3D-Si,[37] resulting in $\alpha_{SC}/\alpha_{3D} \approx 3300$. Namely, the experimental data can be fitted well by

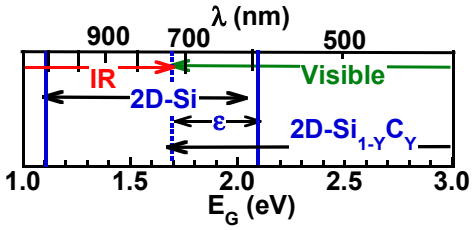

Fig. 14. (Color online) Device design for realizing higher E_G and visible λ_{PL} in a 2D-Si-based semiconductor, where $N_L \geq 4$. Lower and upper axes show E_G and λ_{PL}, respectively. Only the three key parameters of N_L (d_S), $\varepsilon(T_{OX})$, and Y need be considered for realizing various E_G and λ_{PL} in 2D-Si-based devices.

$$\frac{\alpha_{SC}}{\alpha_{3D}} = 6.8 \times 10^4 Y^{1.6}. \tag{6}$$

Consequently, the huge α of 2D-$Si_{1-Y}C_Y$ is possibly caused by the large bandgap modulation by C atoms.

In addition, Fig. 13(b) also shows that the peak I_{PL} even at $E_{EX} = 3.8$ eV drastically increases with increasing Y, similar to the peak I_{PL} excited by the 2.3 eV laser shown in Fig. 13(a), resulting in $I_{PL} \propto Y^{0.9}$ with the correlation coefficient of about 1.

Under both E_{EX} conditions, I_{PL} at $Y = 0.13$, which shows only the C separation effects in Fig. 5(b), is very strong and is about one order of magnitude larger than those for $Y \leq 0.016$. This result suggests that the C phase separation in 2D-Si affects the PL intensity. Consequently, the I_{PL} enhancement in Fig. 13 and the visible λ_{PL} in Figs. 9 and 11 are highly suitable for Si photonics, but it is strongly required to optimize Y and N_L and the C phase separation effects in 2D-$Si_{1-Y}C_Y$.

3.4 Device design for high E_G and visible photon emission

According to the above discussions and our previous works,[6–11] it is possible to increase higher E_G and shorten λ_{PL} of a 2D-Si-based semiconductor by adjusting only the three key parameters of N_L (d_S), strain ε of 2D-Si-based semiconductor with the optimization of the surface SiO_2 thickness T_{OX}, and carbon content Y.

Figure 14 shows the E_G and λ_{PL} design for Si and $Si_{1-Y}C_Y$ alloy semiconductor for $N_L \geq 4$. In the case of band structures with $1.1 < E_G \leq 1.75$ eV and $1000 \leq \lambda_{PL} \leq 700$ nm, E_G monotonically increases and λ_{PL} decreases by decreasing only N_L (d_S) in 2D-Si, because of electron confinement effects in 2D-Si.[6–11] In addition, ε relaxation by thinning T_{OX} of 2D-Si is required to realize the bandgap of $1.75 < E_G \leq 2.1$ eV and $700 < \lambda_{PL} \leq 600$ nm.[11] In particular, in order to realize E_G much higher than 2.1 eV and λ_{PL} shorter than 600 nm, a 2D silicon carbon alloy technology is strongly required, and the Y should be increased. On the other hand, in the case of a heavily doped 2D-silicon-based semiconductor, it is necessary to consider the dopant-induced E_G lowering.[10]

4. Conclusions

We experimentally studied C atom effects on bandgap modulation of a 2D-$Si_{1-Y}C_Y$ layer with a wide range of Y ($4 \times 10^{-5} \leq Y \leq 0.13$) fabricated by the combination of $^{12}C^+$ hot ion implantation into (100)SOI at 900 °C and the following oxidation-induced thinning of the SOI substrate at 900 °C. In

© 2016 The Japan Society of Applied Physics

this study, the minimum atomic layer number of 2D-$Si_{1-Y}C_Y$ was 4. The XPS C-1s spectrum for 2-nm-thick $Si_{0.87}C_{0.13}$ at a C ion dose of $2 \times 10^{16}\,cm^{-2}$ showed the maximum C atomic percent of 13% at the BOX interface, which was also verified by SIMS analysis for an 8.5-nm-thick $Si_{1-Y}C_Y$ layer with the same D_C. Almost all C atoms (about 90%) bound to Si atoms and the C–C bond ratio was only 10%, resulting in a total Si–C atomic percent of about 12% in $Si_{0.87}C_{0.13}$. According to XPS Si-2p and C-1s spectra, about 14% of Si atoms bound to C atoms, whereas 86% of Si atoms was still in Si–Si bonds. By UV-Raman spectroscopy, the Si–C vibration mode peak at $970\,cm^{-1}$ and C–C vibration mode peak at about $1500\,cm^{-1}$ were also confirmed. Thus, we experimentally verified three regions of Si, Si–C, and C in the silicon carbon alloy formed by the C^+ hot ion implantation technique. The C region evaluated by the C–C bond peak in the C-1s spectrum and UV-Raman analysis indicated C atom separation in the $Si_{0.87}C_{0.13}$ layer, but it was not observed for $Y \leq 0.016$.

PL emission was detected in a wide range of $10^{-5} < Y \leq 0.13$, and strongly depended on the excitation laser energy E_{EX}. At high Y ($\geq 0.5\%$), where Si–C and C–C bonds were confirmed by XPS and UV-Raman spectroscopy, we observed a double-peak PL spectrum, and the lower and higher photon energy peaks were attributable to Si and Si–C regions in the 2D $Si_{1-Y}C_Y$ alloy, respectively. E_{PH} excited by the 3.8 eV laser was almost independent of Y, and E_{PH} of 2.5 eV and visible λ_{PL} of 500 nm were achieved at $Y = 0.13$. Thus, the C phase separation at $Y = 0.13$ did affect E_{PH}. On the other hand, at low Y ($< 2\%$), the E_{PH} increase was well explained by the C-atom-induced compressive strain in 2D-$Si_{1-Y}C_Y$. I_{PL} of 2D-$Si_{1-Y}C_Y$ rapidly increased with increasing Y, which was probably due to the much larger absorption coefficient than that of 2D-Si. The very large I_{PL} at $Y = 0.13$ might be caused by the C atom separation.

Consequently, we can precisely design a future CMOS-SHOT and photonics composed of 2D-Si-based semiconductors with various high E_G and visible λ_{PL} by controlling only the three parameters of Si atom layer number N_L (d_S), strain ε (T_{OX}) which depends on the surface oxide thickness T_{OX}, and carbon content Y.

Acknowledgements

We would like to thank Professor J. Nakata and Dr. Y. Hoshino of Kanagawa University for support during the carbon ion implantation.

1) J.-P. Colinge, *Silicon-on-Insulator Technology* (Kluwer, Dordrecht, 2004).
2) T. Irisawa, T. Numata, T. Tezuka, K. Usuda, S. Sugiyama, and S. Takagi, IEEE Trans. Electron Devices **55**, 649 (2008).
3) S. Saito, D. Hisamoto, H. Shimizu, H. Hamamura, R. Tsuchiya, Y. Matsui, T. Mine, T. Arai, N. Sugii, K. Torii, S. Kimura, and T. Onai, Jpn. J. Appl. Phys. **45**, L679 (2006).
4) S. Saito, N. Sakuma, Y. Suwa, H. Arimoto, D. Hisamoto, H. Uchiyama, J. Yamamoto, T. Sakamizu, T. Mine, S. Kimura, T. Sugawara, M. Aoki, and T. Onai, IEDM Tech. Dig., 2008, 19.5.
5) L. Pavesi and D. J. Lockwood, *Silicon Photonics* (Springer, Berlin, 2004).
6) T. Mizuno, K. Tobe, Y. Maruyama, and T. Sameshima, Jpn. J. Appl. Phys. **51**, 02BC03 (2012).
7) T. Mizuno, T. Aoki, Y. Nagata, Y. Nakahara, and T. Sameshima, Jpn. J. Appl. Phys. **52**, 04CC13 (2013).
8) T. Mizuno, Y. Nakahara, Y. Nagata, Y. Suzuki, T. Aoki, and T. Sameshima, Jpn. J. Appl. Phys. **53**, 04EC08 (2014).
9) T. Mizuno, Y. Nagata, Y. Suzuki, Y. Nakahara, T. Aoki, and T. Sameshima, Jpn. J. Appl. Phys. **53**, 04EC09 (2014).
10) T. Mizuno, Y. Nagamine, Y. Suzuki, Y. Nakahara, Y. Nagata, T. Aoki, and T. Sameshima, Jpn. J. Appl. Phys. **54**, 04DC05 (2015).
11) T. Mizuno, Y. Suzuki, Y. Nagamine, Y. Nakahara, Y. Nagata, T. Aoki, and T. Maeda, Jpn. J. Appl. Phys. **54**, 04DC02 (2015).
12) N. Fukata, T. Oshima, K. Murakami, T. Kizuka, T. Tsurui, and S. Ito, J. Appl. Phys. **100**, 024311 (2006).
13) K. W. Adu, H. R. Gutierrez, and P. C. Eklund, in *Nanosilicon*, ed. V. Kumar (Elsevier, Amsterdam, 2008) Chap. 7.
14) H. Richter, Z. P. Wang, and L. Ley, Solid State Commun. **39**, 625 (1981).
15) I. H. Campbell and P. M. Fauchet, Solid State Commun. **58**, 739 (1986).
16) K. Uchida, H. Watanabe, A. Kinoshita, J. Koga, T. Numata, and S. Takagi, IEDM Tech. Dig., 2002, p. 47.
17) K. Uchida, J. Koga, and S. Takagi, J. Appl. Phys. **102**, 074510 (2007).
18) G. Tsutsui, M. Saitoh, and T. Hiramoto, IEEE Trans. Electron Devices **26**, 836 (2005).
19) L. Donetti, F. Gámiz, J. B. Roldán, and A. Godoy, J. Appl. Phys. **100**, 013701 (2006).
20) B. K. Agrawal and S. Agrawal, Appl. Phys. Lett. **77**, 3039 (2000).
21) M. Tabe, M. Kumezawa, and Y. Ishikawa, Jpn. J. Appl. Phys. **40**, L131 (2001).
22) Z. H. Lu and D. Grozea, Appl. Phys. Lett. **80**, 255 (2002).
23) S. S. Iyer and Y.-H. Xie, Science **260**, 40 (1993).
24) Y. Takahashi, T. Furuta, Y. Ono, T. Ishiyama, and M. Tabe, Jpn. J. Appl. Phys. **34**, 950 (1995).
25) H. Omi, T. Kawamura, S. Fujikawa, Y. Tsusaka, Y. Kagoshima, and J. Matsui, Appl. Phys. Lett. **86**, 263112 (2005).
26) S. M. Sze and K. K. Ng, *Physics of Semiconductor Devices* (Wiley, New York, 2007).
27) T. Mizuno, N. Sugiyama, T. Tezuka, Y. Moriyama, S. Nakaharai, T. Maeda, and S. Takagi, IEEE Trans. Electron Devices **52**, 2690 (2005).
28) T. Mizuno, Y. Moriyama, T. Tezuka, N. Sugiyama, and S. Takagi, Jpn. J. Appl. Phys. **50**, 010107 (2011).
29) K.-J. Chui, K.-W. Ang, N. Balasubramanian, M.-F. Li, G. S. Samudra, and Y.-C. Yeo, IEEE Trans. Electron Devices **54**, 249 (2007).
30) L. R. Tessler and I. Solomon, Phys. Rev. B **52**, 10962 (1995).
31) W. Liu, M. Zhang, C. Lin, Z. Zeng, L. Wang, and P. K. Chu, Appl. Phys. Lett. **78**, 37 (2001).
32) S. T. Pantelides and S. Zollner, *Silicon-Germanium Carbon Alloys* (Taylor & Francis, New York, 2002).
33) T. Mizuno, Y. Nagamine, Y. Omata, Y. Suzuki, W. Urayama, T. Aoki, and T. Sameshima, Ext. Abstr. Solid State Devices and Materials, 2015, p. 1138.
34) T. Mizuno, M. Hasegawa, K. Ikeda, M. Nojiri, and T. Horikawa, Jpn. J. Appl. Phys. **50**, 04DC02 (2011).
35) Web [http://www.soitec.com/en/].
36) D. N. Talwar and Z. C. Feng, Comput. Mater. Sci. **30**, 419 (2004).
37) T. Mizuno, Y. Nagata, Y. Suzuki, Y. Nakahara, T. Tanaka, T. Aoki, and T. Sameshima, Ext. Abstr. Solid State Devices and Materials, 2013, p. 96.

 © 2016 The Japan Society of Applied Physics